Electronic Supplementary Material (ESI) for Journal of Materials Chemistry C.

Tunable 3D light trapping architectures based on self-assembled $SnSe_2$ nanoplate arrays for ultrasensitive SERS detection

Weiwei Li,[1,2#] Lei Xiong,[1,3#] Nianci Li,[1,4] Shuo Pang,[1,2] Guoliang Xu,[1,2] Chenghan Yi,[1,2] Zhixun Wang,[5] Guoqiang Gu,[6] Kaiwei Li,[7] Weimin Li,[1] Lei Wei,[4] Guangyuan Li,[1]* Chunlei Yang,[1]* and Ming Chen[1]*

[1]*Shenzhen Institutes of Advanced Technology, Chinese Academy of Sciences, Shenzhen 518055, People's Republic of China*
[2]*Department of Nano Science and Technology Institute, University of Science and Technology of China, Suzhou 215123, People's Republic of China*
[3]*School of Information Science and Engineering, Yunnan University, Yunnan 650500, People's Republic of China*
[4]*School of Computer and Control Engineering, University of Chinese Academy of Sciences, Beijing 100049, People's Republic of China*
[5]*School of Electrical and Electronic Engineering, Nanyang Technological University, 50 Nanyang Avenue, 639798, Singapore*
[6]*Department of Electrical and Electronic Engineering, Southern University of Science and Technology, Shenzhen, 518055, People's Republic of China*
[7]*Guangdong Provincial Key Laboratory of Optical Fiber Sensing and Communications, Institute of Photonics Technology, Jinan University, Guangzhou, 510632, People's Republic of China*

[*]*email: gy.li@siat.ac.cn; cl.yang@siat.ac.cn; ming.chen2@siat.ac.cn*

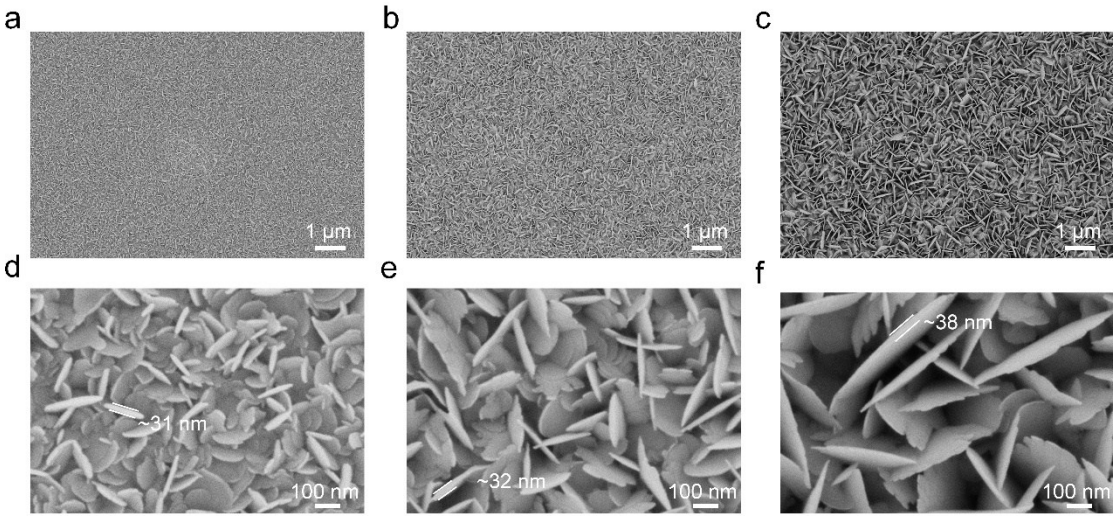

Figure S1. (a-c) Representative top-view SEM images of the resulting $SnSe_2$ NPAs, corresponds to a certain deposition time (5, 10 and 20 min, respectively). (d-f) Representative top-view SEM images of the resulting $SnSe_2$ NPAs, corresponds to a certain deposition time (5, 10 and 20 min, respectively). The thickness of the $SnSe_2$ NPAs is about 30~40 nm (> 10 layers, bulk).

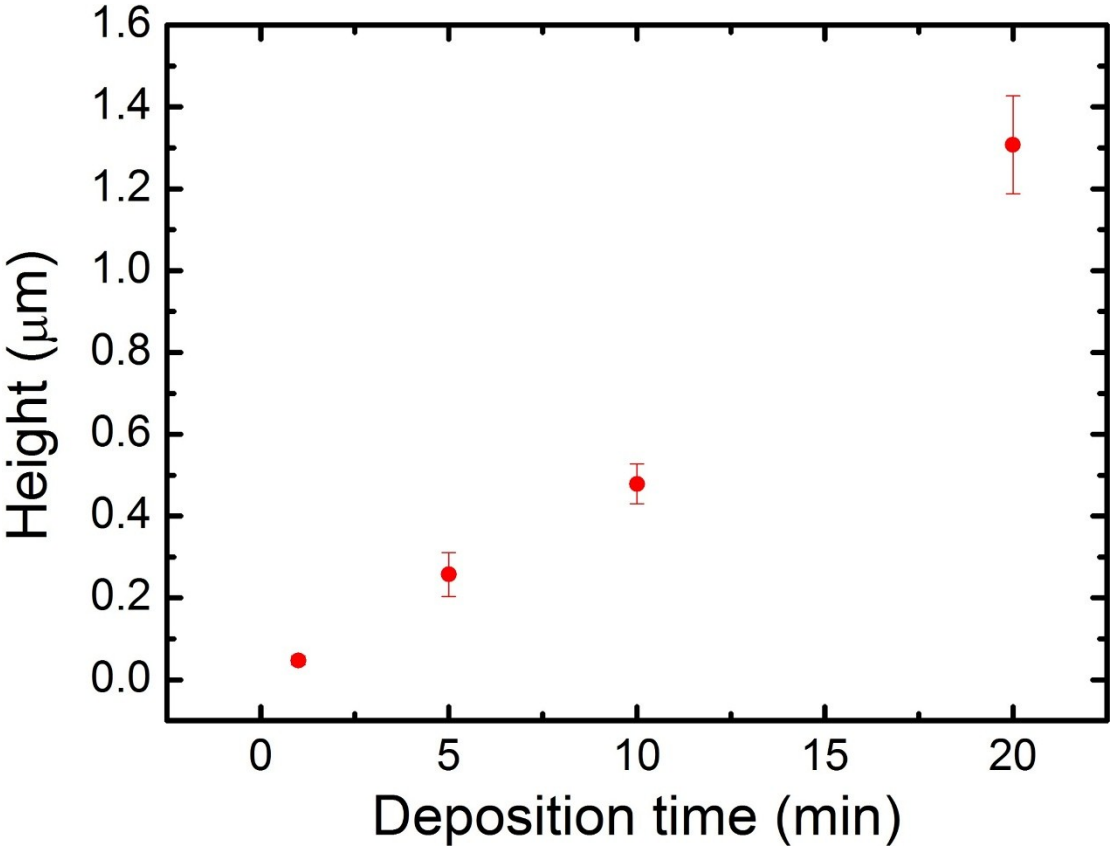

Figure S2. Height of $SnSe_2$ NPAs as a function of deposition time.

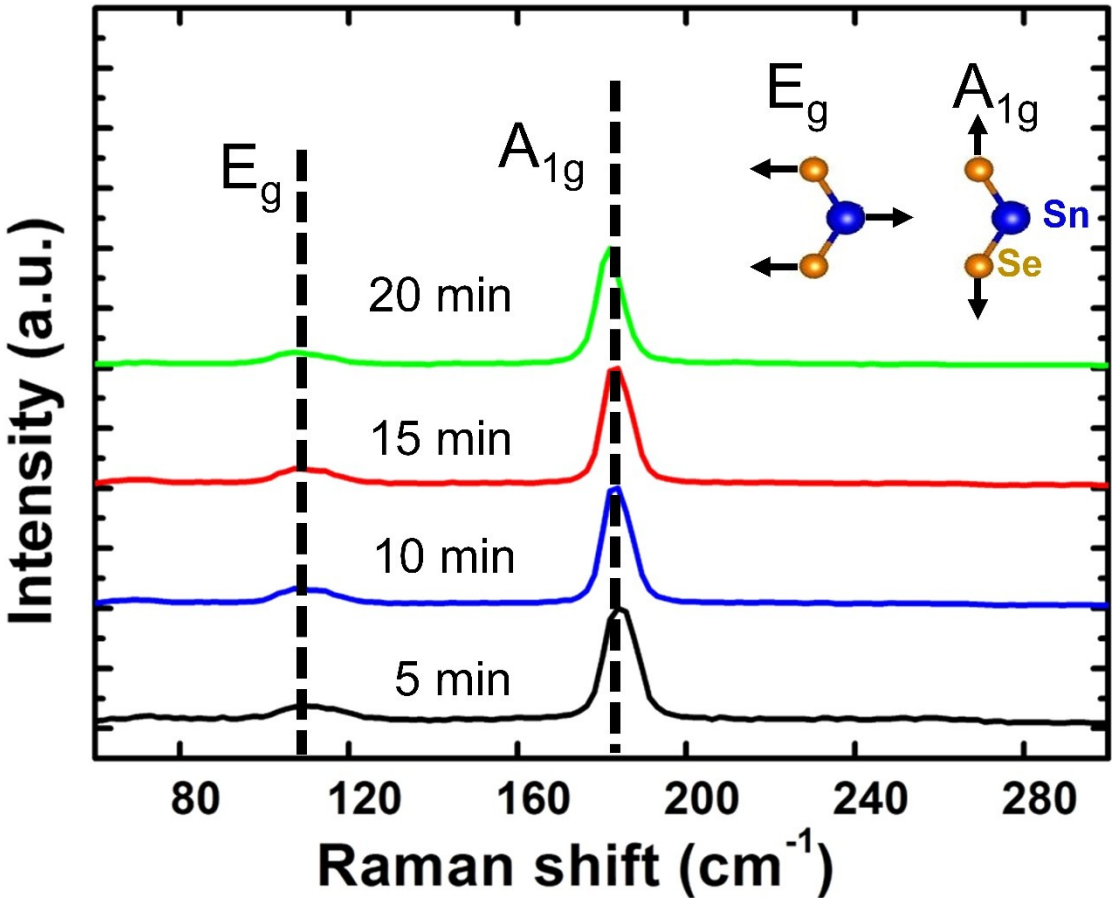

Figure S3. Raman spectra of $SnSe_2$ NPAs with different deposition time.

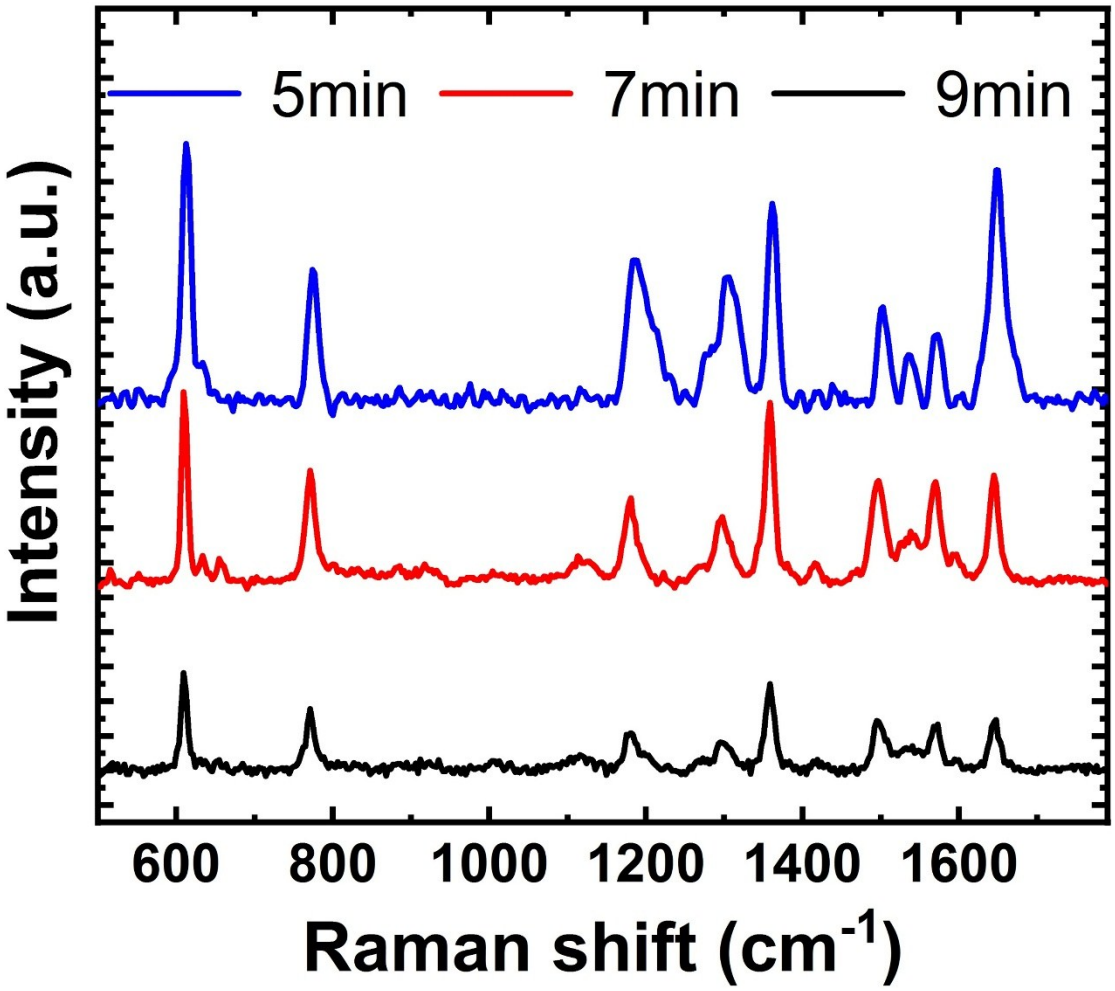

Figure S4. SERS spectra of R6G (10^{-6} M) adsorbed on $SnSe_2$ NPAs with different deposition time.

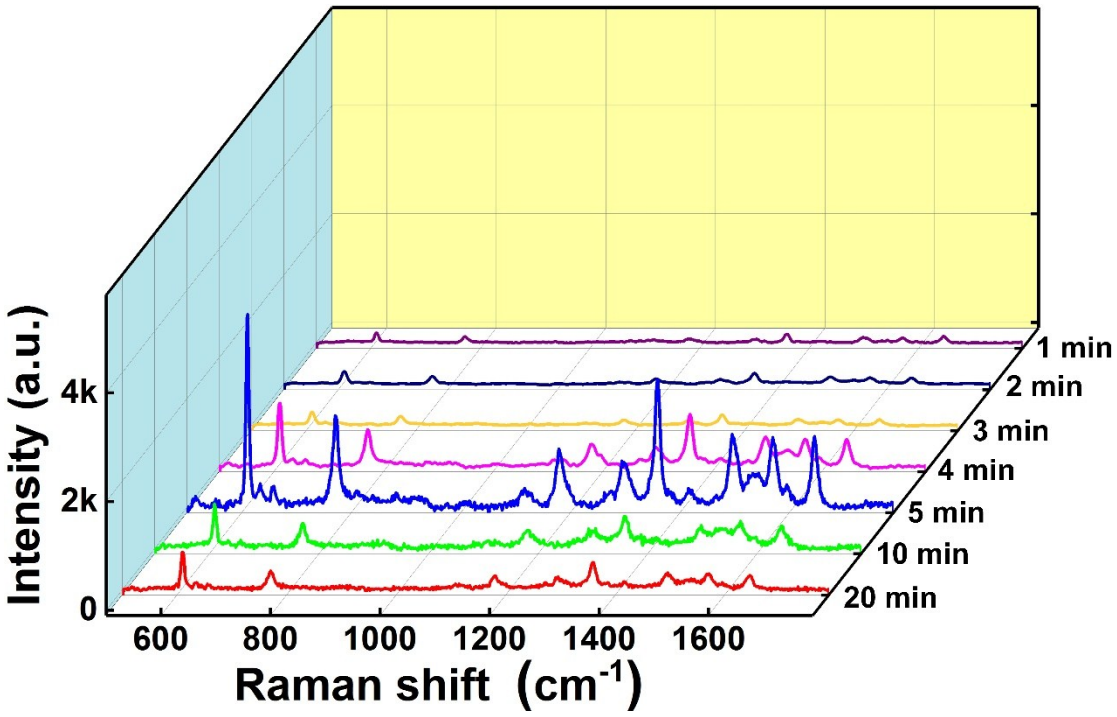

Figure S5. SERS spectra of R6G (10^{-6} M) adsorbed on $SnSe_2$ NPAs (another batch of samples) with different deposition time. The result indicates the highly reproductive feature, compared with the results shown in Figure 3a.

Charge-transfer process

The valence band (VB) and the conduction band (CB) of $SnSe_2$ were calculated by the following equations (S1) and (S2) [1]

$$E_c = -(\chi(A)^a * \chi(B)^b * \chi(C)^c)^{1/(a+b+c)} + 1/2E_g \quad \text{(S1)}$$

$$E_v = E_c + E_g \quad \text{(S2)}$$

where E_v and E_c are the valence band and conduction band edge, respectively. χ is the electronegativity of the semiconductor, which is geometric mean of the electronegativity of the constituent atoms. For $SnSe_2$, the value of bandgap E_g was calculated to be 1.2 eV by the following equation (S3)[2]

$$E_g = 1240/\lambda_{abs} \quad \text{(S3)}$$

where λ_{abs} is 1028 nm, as required from the photoluminescence spectra shown Figure S6a. Thus, the E_v and E_c of $SnSe_2$ was -4.7 eV and -3.5 eV, respectively. Figure S6b depicts the charge-transfer process at the interface between R6G proble molecule and $SnSe_2$. The valence band (VB) (−4.7 eV) and conduction band (CB) (−3.5 eV) of $SnSe_2$ are located between the HOMO (-5.70 eV) and LUMO (-3.40 eV). The vibronic coupling between $SnSe_2$ (CB state |S> and VB state |S′>) and R6G molecule (excited state |K> and ground state |I>) leads to the charge transfer process. Considering of the excitation energy and R6G molecule, when a laser with wavelength of 532 nm was used, the following transfer processes can occur according to the energy level relationship [3] : (1) ($T_{S'S}$), (2) (T_{IK}), (3) ($T_{S'K}$), (4) (T_{IS}), (5) ($T_{IS'}$) and (6) (T_{SK}), which are shown in Figure S6b. Attributing to enormous enhancement of the polarizability of the R6G molecule, recombination of electrons and holes is increasing, which enhances the peak intensity of R6G molecules.

In additional, for the two dimensional $SnSe_2$ nanomaterials, the large specific surface area will also benefit to the easier combination of surface atoms (Sn, Se) with adsorbed R6G molecules, in turn leading to stronger photoinduced charge-transfer process [4].

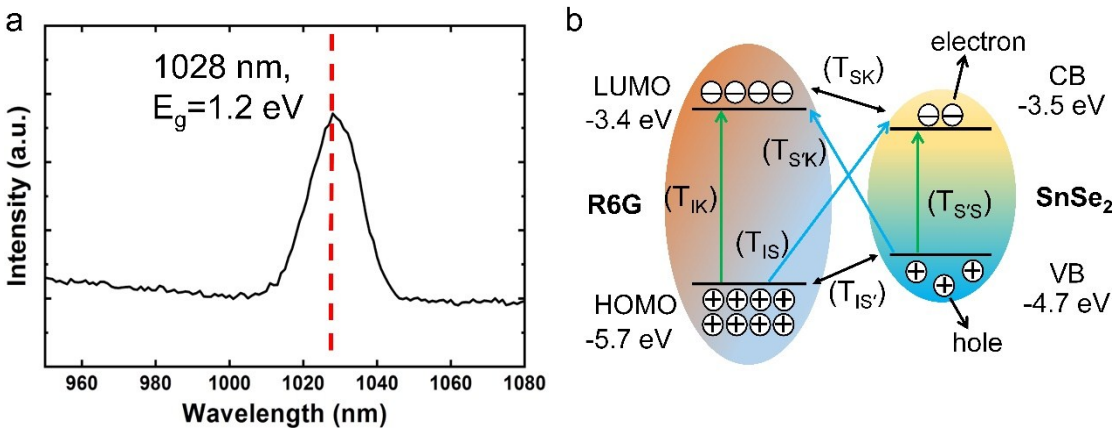

Figure S6. (a) Photoluminecence spectra of $SnSe_2$ NPAs. (b) Schematic illustration of the photoinduced charge-transfer process between $SnSe_2$ NPAs and R6G under the excitation of 532 nm.

Calculation of enhancement factor (EF)

The Raman enhancement factor (EF) of as-fabricated $SnSe_2$ NPAs SERS substrate was calculated by the following equation (S4) [5]:

$$EF = (I_{SERS} / N_{SERS}) / (I_{NR} / N_{NR}) \quad \text{(S4)}$$

In equation S4, I_{SERS} and I_{NR} are the Raman intensity of normal Raman signal collected from probe molecule adsorbed on $SnSe_2$ NPAs (1cm×1cm) and normal Raman signal collected from probe molecule (0.1 M) drop on rectangular glass (1cm×1cm), respectively. N_{SERS} and N_{NR} are the amounts of molecules involved in the SERS experiments and estimated for 100 μL of the aqueous solution of probe molecule (0.1 M) dropped on a glass which produced a deposition area about $1cm^2$ (1cm×1cm), respectively. Here we use R6G probe molecules and 611 cm^{-1} peak to calculate the EF.

The amounts of the detected molecule N_{SERS} can be calculated by:

$$N_{SERS} = CV_{solution}S_{spot}N_A / S_{sub} \quad \text{(S5)}$$

where C is the concentration of probe molecule, $V_{solution}$ is the volume of used probe molecules drop, S_{spot} and S_{sub} are the area of laser spot and the area of rectangular glass substrate ($1cm^2$), respectively, N_A is Avogadro constant (6.22×10^{23}). The laser spot diameter d ($d = 1.22\lambda_{laser} / N_A$, λ_{laser} is the incident wavelength 532 nm, the numerical aperture of the objective lens N_A = 0.5) is about 1.3 μm. Thus, the laser spot area $S_{spot} = \pi(d/2)^2$ is about 1.33 μm^2.

The Raman 611 cm^{-1} intensity of R6G/$SnSe_2$ NPAs (1×10^{-10} M) is 35.6 counts (Figure S7b) with 10 s acquisition time, and that of bulk R6G is 562.5 counts with 1 s acquisition time (Figure S7a). With normalization in case of acquisition time, the Raman intensity ratio is estimated to be I_{SERS} / I_{NR} = (35.6/10)/(562.5)=6.33×10^{-3}. Therefore, according to the equation (S4) and (S5), the EF of as-fabricated $SnSe_2$ NPAs SERS substrate was calculated to be $EF = (6.33\times10^{-3})(10^{-1} / 10^{-10})$ =6.33×10^6.

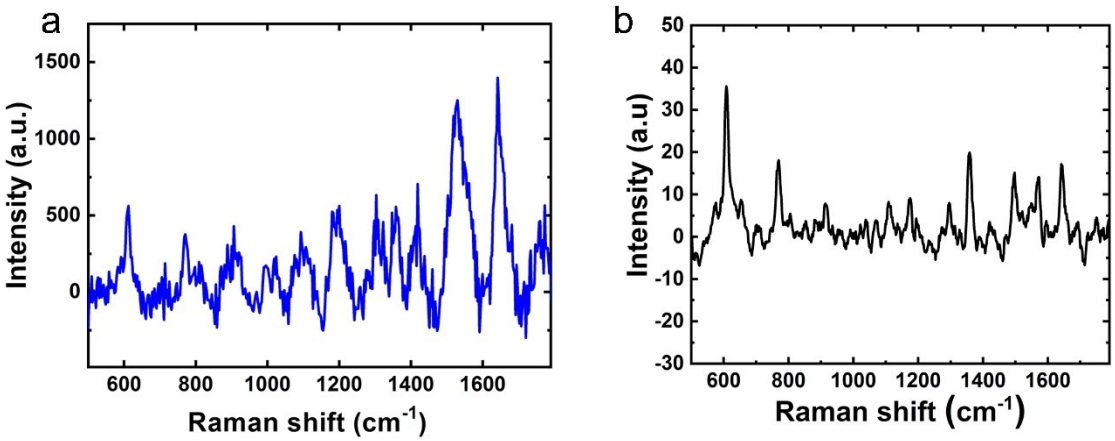

Figure S7. (a) SERS spectra of R6G (0.1 M) adsorbed on glass substrate (1 s acquisition time). (b) SERS spectra of R6G (1×10^{-10} M) adsorbed on glass substrate (10 s acquisition time).

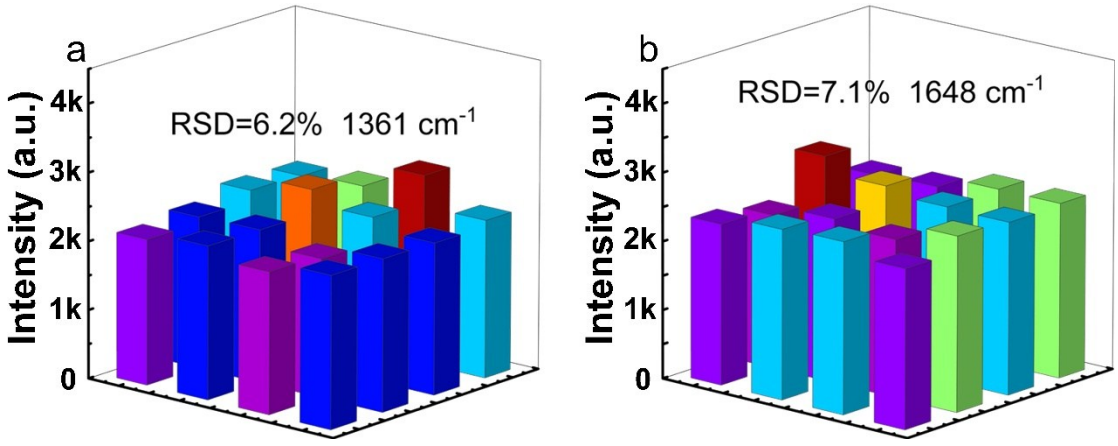

Figure S8. The Raman intensities of R6G at peak of 1361 cm^{-1} and 1648 cm^{-1}, acquired from SERS spectra shown in Figure 4a.

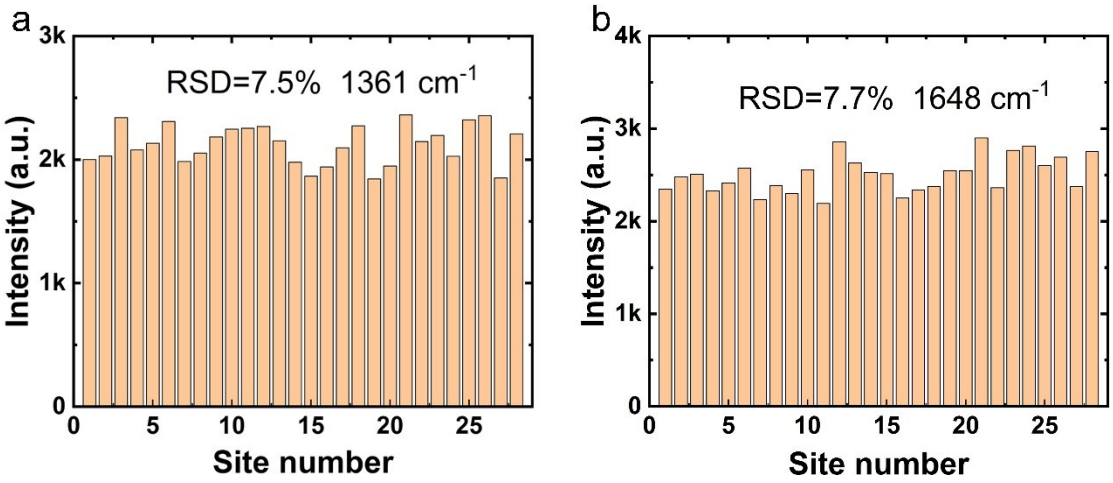

Figure S9. The Raman intensities of R6G at peak of 1361 cm^{-1} and 1648 cm^{-1}, acquired from SERS spectra shown in Figure 4c.

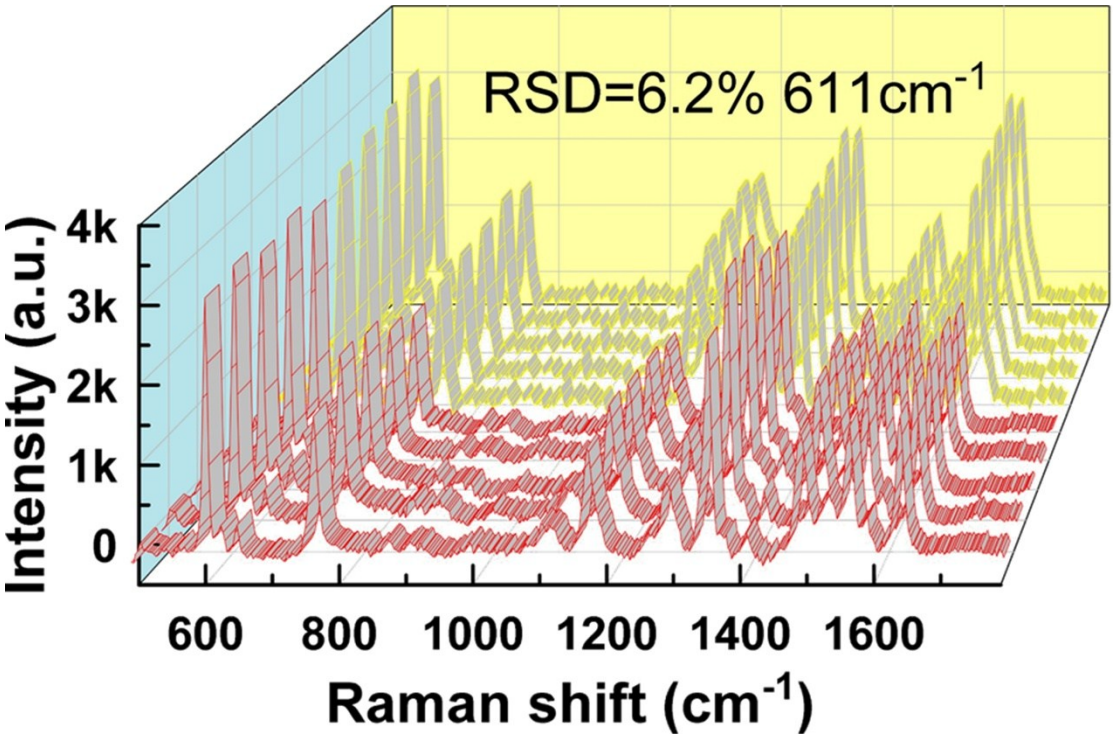

Figure S10. Sample to sample Raman intensity variations. 5 SERS spectra (yellow line) and 5 SERS sepctra (red lines) are collected from different samples. A small sample-to-sample RSD of 6.2% was achieved.

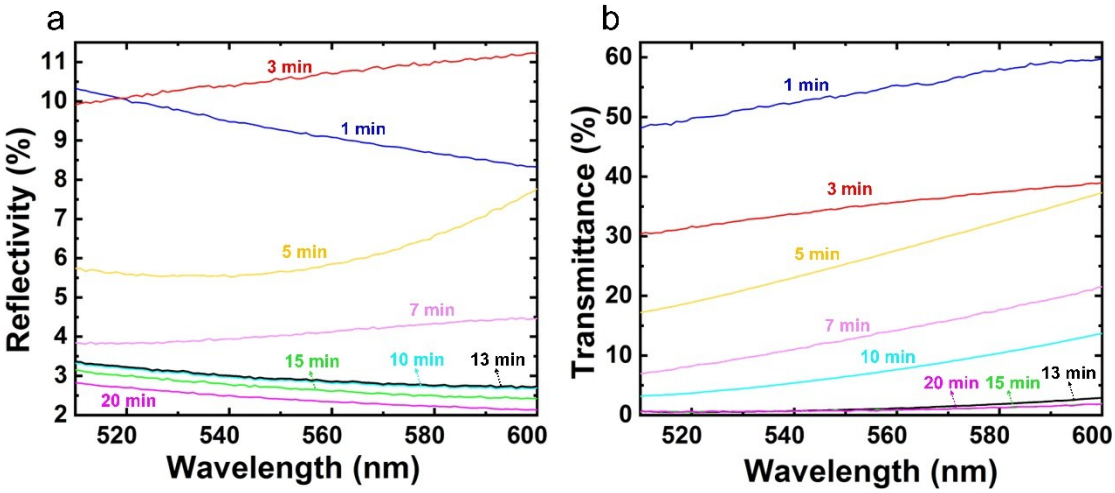

Figure S11. (a) Measured reflectivity of $SnSe_2$ NPAs with different deposition time. (b) Measured transmittance of $SnSe_2$ NPAs with different deposition time.

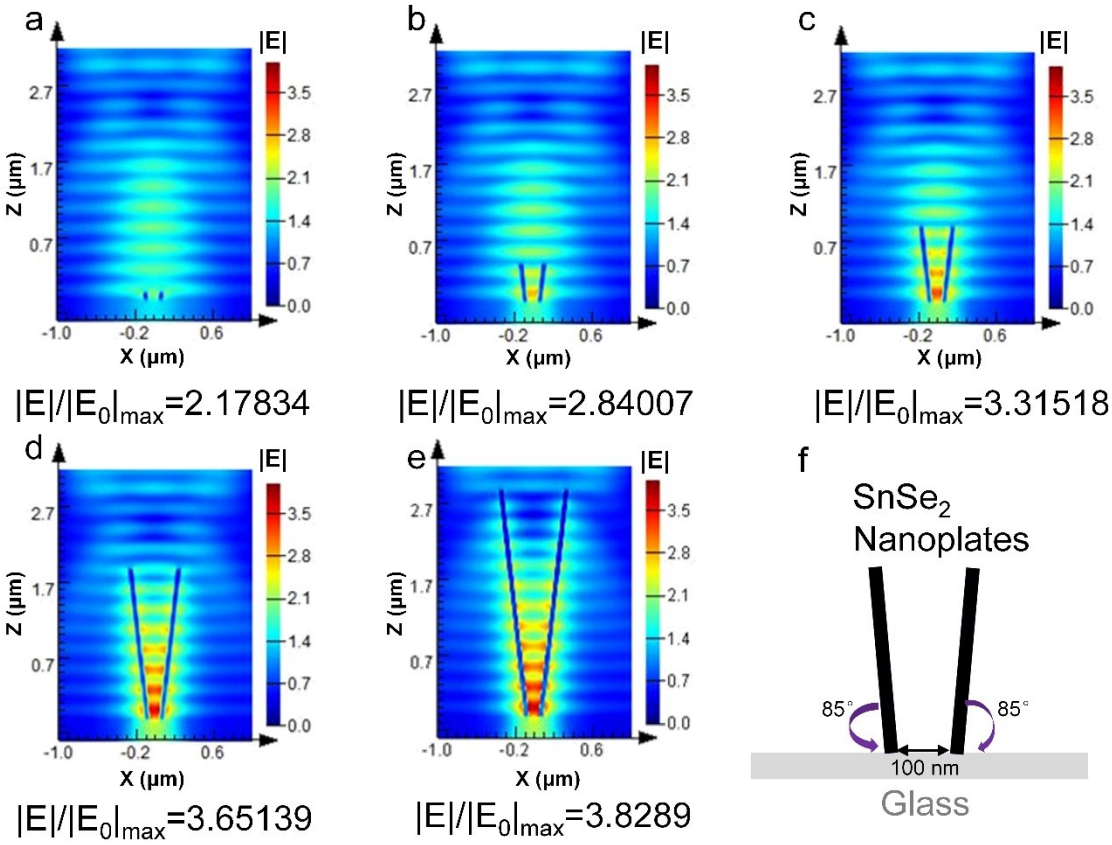

Figure S12. (a-e) Calculated electric field ($|E|/|E_0|$) distributions of $SnSe_2$ NPAs with different heights. (f) Schematic diagram of the modeled structure (symmetric structure, with 85° angle for both nanoplates).

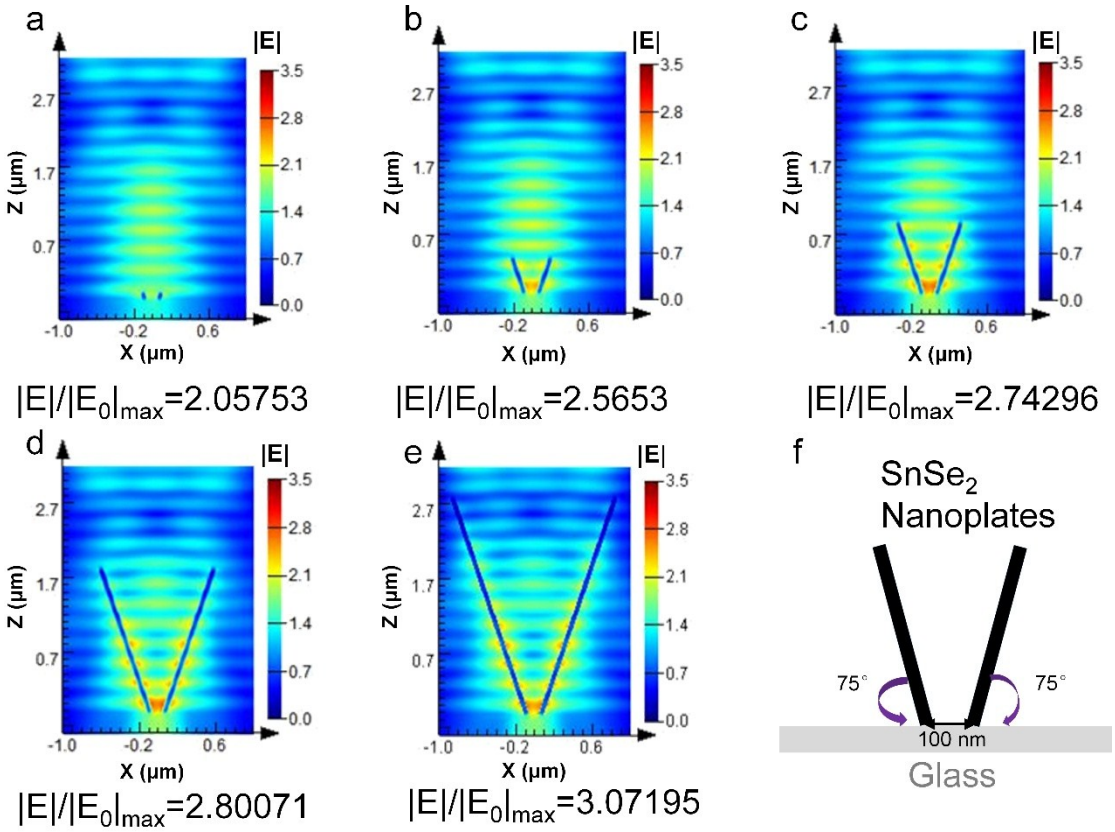

Figure S13. (a-e) Calculated electric field ($|E|/|E_0|$) distributions of $SnSe_2$ NPAs with different heights. (f) Schematic diagram of the modeled structure (symmetric structure, with 75° angle for both nanoplates).

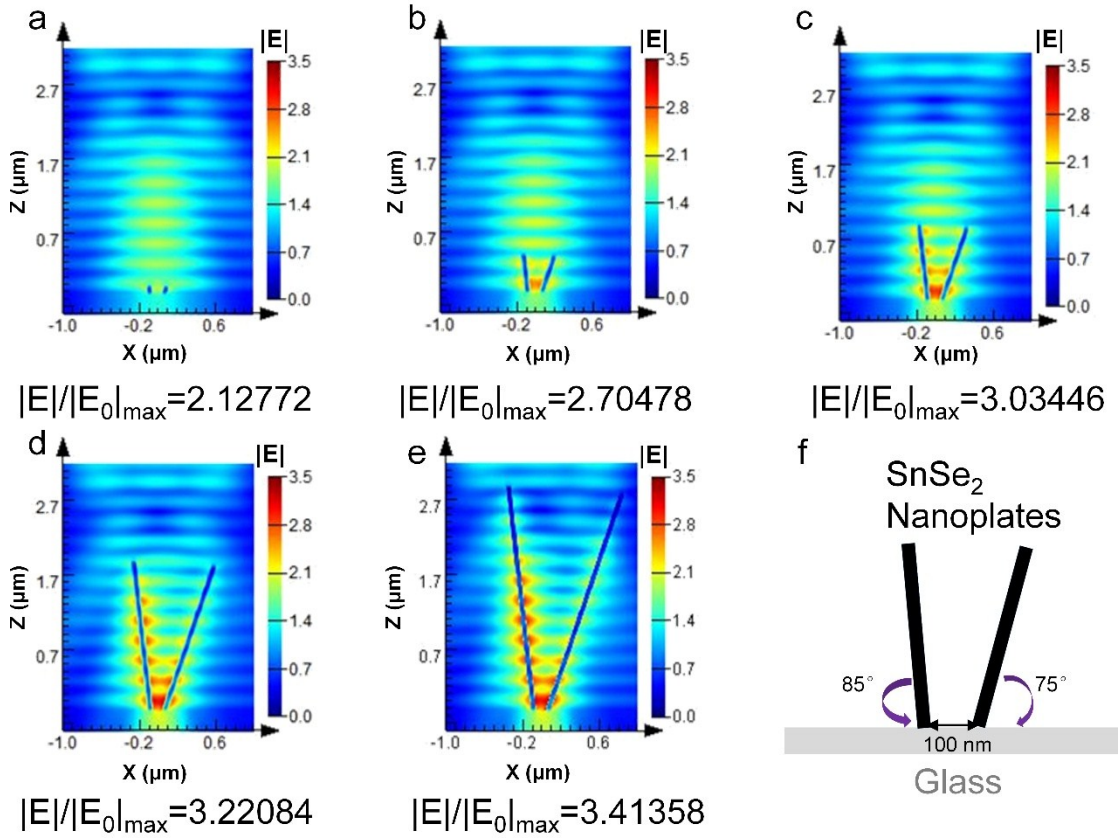

Figure S14. (a-e) Calculated electric field ($|E|/|E_0|$) distributions of $SnSe_2$ NPAs with different heights. (f) Schematic diagram of the modeled structure (asymmetric structure, with 85° angle for the left nanoplate and 75° angle for the right nanoplate).

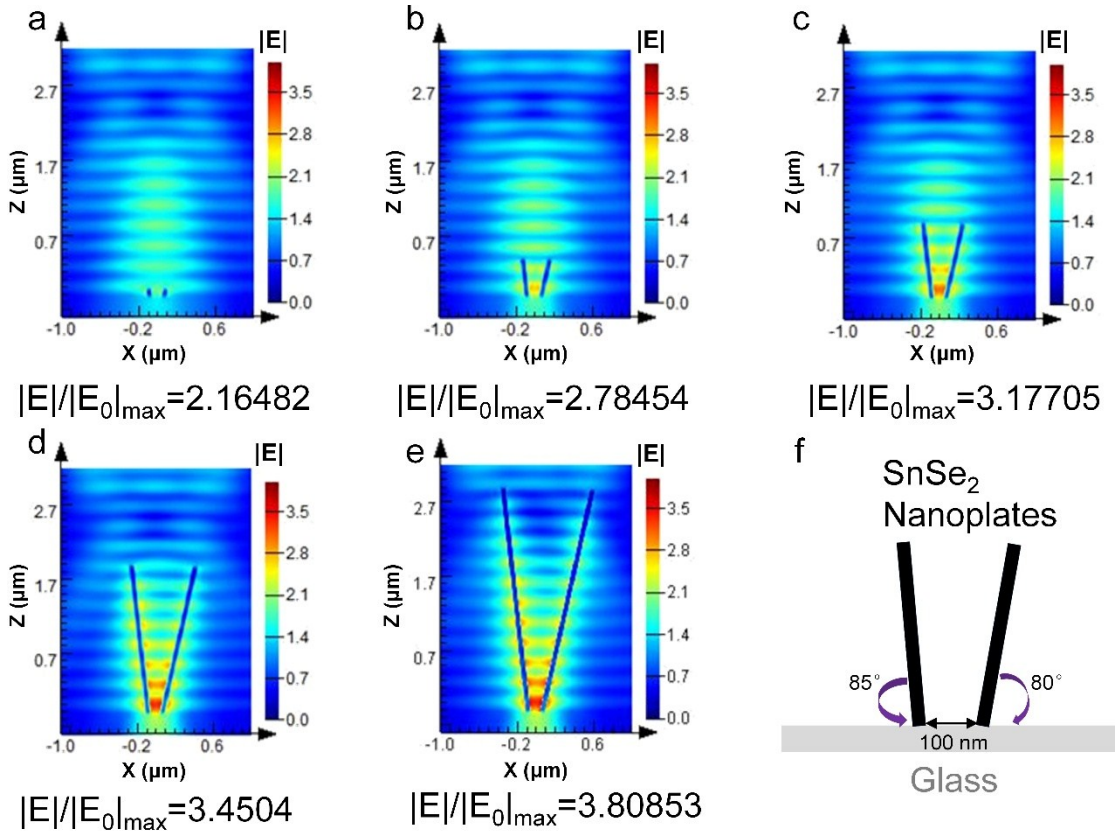

Figure S15. (a-e) Calculated electric field ($|E|/|E_0|$) distributions of $SnSe_2$ NPAs with different heights. (f) Schematic diagram of the modeled structure (asymmetric structure, with 85^o angle for the left nanoplate and 80^o angle for the right nanoplate).

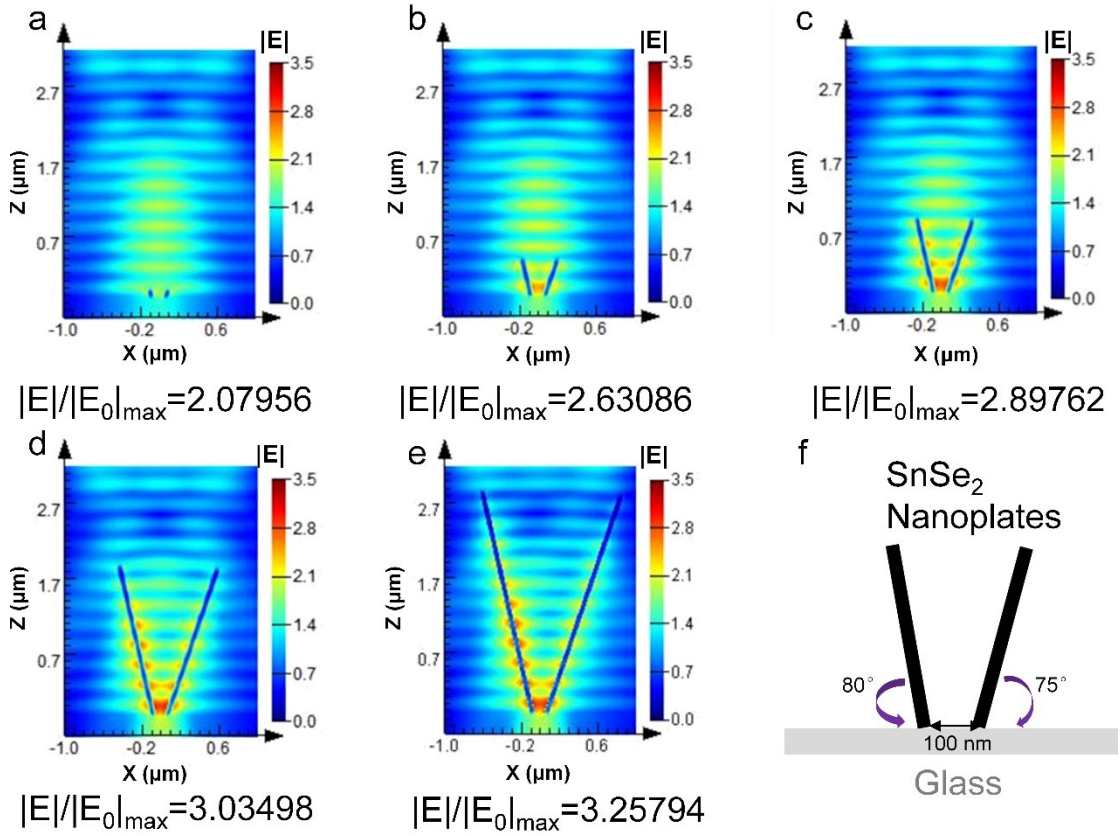

Figure S16. (a-e) Calculated electric field ($|E|/|E_0|$) distributions of $SnSe_2$ NPAs with different heights. (f) Schematic diagram of the modeled structure (asymmetric structure, with 80° angle for the left nanoplate and 75° angle for the right nanoplate).

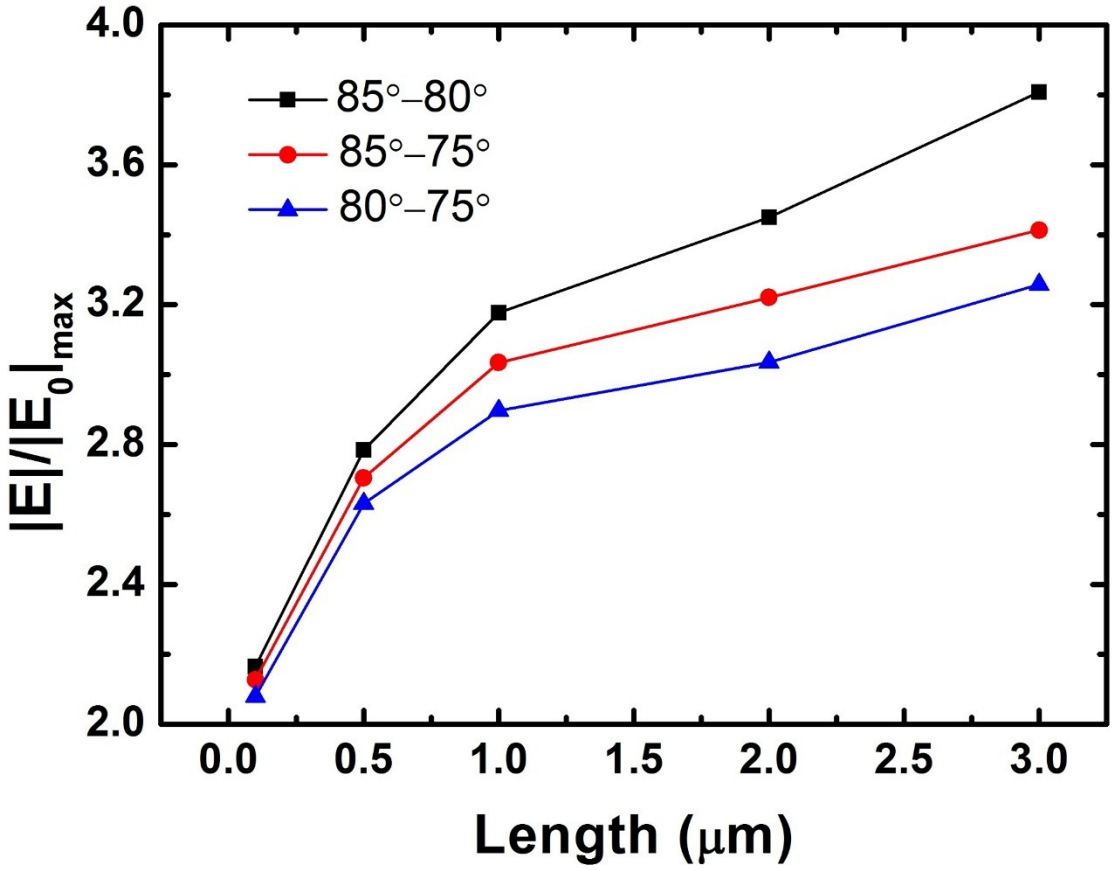

Figure S17. The calculated maximum intensity $|E|/|E_0|$ of $SnSe_2$ NPAs with different heights and angles (asymmetric structure)

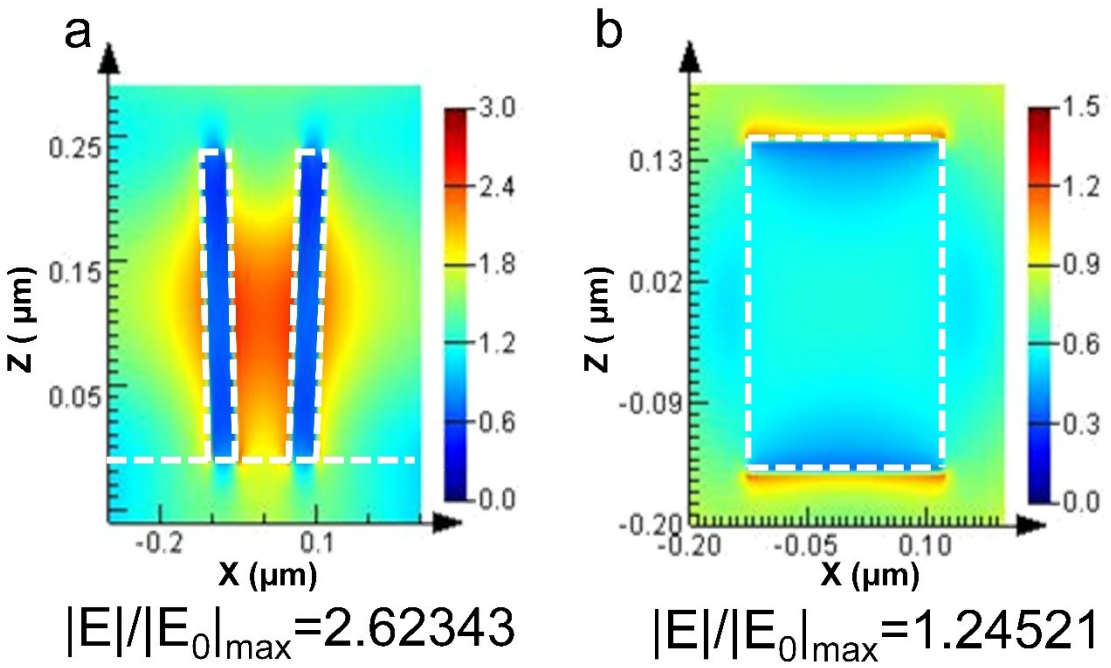

Figure S18. (a-b) Calculated electric field ($|E|/|E_0|$) distributions for vertical-structured $SnSe_2$ NPAs (*t*=5 min, height=0.25 μm, width=0.3 μm, thickness=35 nm) and tiled $SnSe_2$ nanoplate (*t*=1 min, thickness=35 nm, length= 0.25 μm, width=0.3μm), respectively.

Enhanced SERS performance *via* inserting high reflective layer-Distributed Bragg Reflectors (DBR)

We use Ta_2O_5/SiO_2 DBR as the high reflective layer. The n, k value of Ta_2O_5 are 2.1469 and 0.00081579 for 532 nm (laser wavelength), respectively. The n value of SiO_2 is 1.46 for 532 nm. Then the thickness of the Ta_2O_5 and SiO_2 layer can be obtained by the following equation[6]:

$$L = \frac{\lambda_{Bragg}}{4n} \tag{S6}$$

where L is the thickness of the layer, λ_{Bragg} is the Bragg central wavelength (532 nm). The calculated thickness of of the Ta_2O_5 and SiO_2 layer are 62 nm and 91 nm, respectively. The reflectivity R of the DBR can then be obtained by the following equation[6]:

$$R = \left(\frac{1-(n_{Ta_2O_5}/n_{SiO_2})^{2m}}{1+(n_{Ta_2O_5}/n_{SiO_2})^{2m}}\right)^2 \tag{S7}$$

where m is the pairs of Ta_2O_5/SiO_2. The result is shown in Figure S18a, the reflectivity of the Ta_2O_5/SiO_2 DBR (10 pairs) is 0.998 (close to 100%).

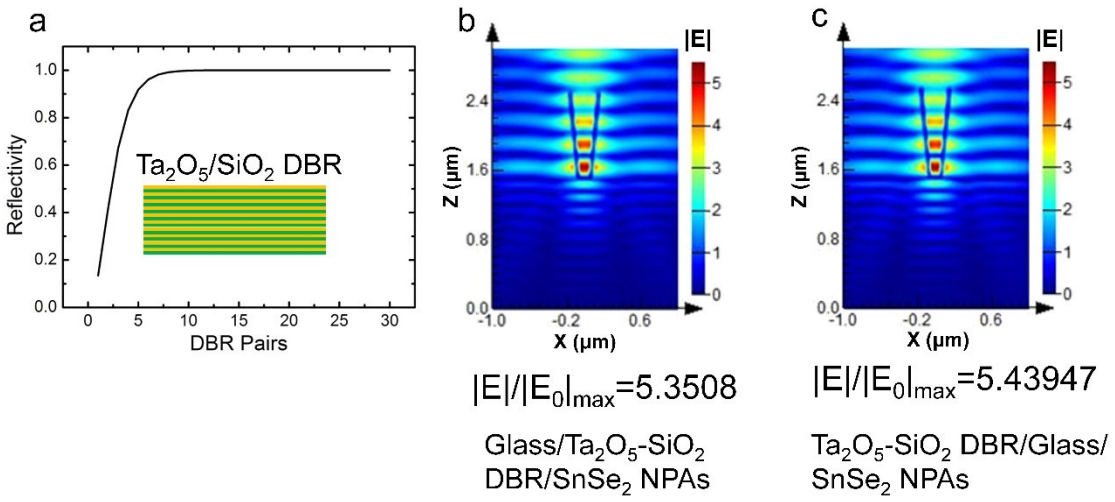

Figure S19. (a) Calculated reflectivity of Ta_2O_5/SiO_2 DBR as a function of DBR pairs. (b-c) The electric field ($|E|/|E_0|$) distributions of Glass/Ta_2O_5-SiO_2 DBR/$SnSe_2$ NPAs scheme and Ta_2O_5-SiO_2 DBR/Glass/$SnSe_2$ NPAs scheme (10 pairs DBR symmetric structure, length of $SnSe_2$ NPAs=1 μm, angle=85°, thickness of Glass=50 nm). Compared to the results shown in Figure S12c, the maximum intensity $|E|/|E_0|$ increases from 3.32 to 5.35 (5.44), which can promote the coupling between the incident light and $SnSe_2$ NPAs, in turn enhance the SERS performance.

Table S1: Summary of semiconductors and noble metals SERS activity

Material	Analyte	EF	LOD(M)	Laser	Ref.
$SnSe_2$ NPAs	R6G	$6.33x10^6$	$1x10^{-12}$	532nm	This work
$SnSe_2$ Nanoflakes (isolated flakes)	R6G	-	$1x10^{-8}$	532nm	[3]
Cu_2O Concave Sphere（single particle）	CV and R6G	$2.8x10^5$ (CV), $2.5x10^5$ (R6G),	$2x10^{-8}$	647nm	[7]
TiO_2 microarrays	Methylene Blue	$2x10^4$	$6x10^{-6}$	532nm	[8]
SiO_2@TiO_2 core-shell spheres	Methylene Blue	-	$1x10^{-5}$	633nm	[9]
Au@SiO_2	R6G	$1x10^6$	$1x10^{-9}$	785nm	[10]
Cu_2O Nanospheres	4-MBA	$1x10^5$	$1x10^{-3}$	488nm	[11]
Bulk MoS_2	R6G	$1.9x10^6$	$1x10^{-8}$	532nm	[12]
3D-stacked Ag NWs	Methylene Blue	-	$1.5x10^{-9}$	632.8nm	[13]
AuNPs@MoS_2	R6G	$8.2x10^5$	$1x10^{-6}$	633nm	[14]
3D TiO_2 nanofibers	CV	$1.3x10^6$	-	532nm	[15]

References:

1. P. Y. Ma, H. J. Yu, Y. Yu, W. M. Wang, H. Wang, J. Y. Zhang, Z. Y. Fu, *Phys. Chem. Chem. Phys.* **2016**, *18*, 3638–3643
2. J. Tauc, R. Grigorovici, A. Vancu, *Phys. Status Solidi* **1966**, *15*, 627
3. Y. Zhang, Y. Shi, M. Wu, K. Zhang, B. Man, M. Liu, *Nanomaterials* **2018**, *8*, 515.
4. C. Muehlethaler, C. R. Considine, V. Menon, W. C. Lin, Y. H. Lee, J. R. Lombardi, *ACS Photonics* **2016**, *3*, 1164.
5. J. Huang, D. Ma, F. Chen, M. Bai, K. Xu and Y. Zhao, *Anal. Chem.* **2015**, *87*, 10527.
6. C. Wilmsen, H. Temkin, L. A. Coldren, "Vertical cavity surface emitting lasers: design, fabrication, characterization and applications [M]," *Cambridge Studies in Modem Optics*. **2001**, 24, pp. 73.
7. X. X. Li, Y. Shang, J. Lin, A. R. Li, X. T. Wang, B. Li, L. Guo, *Adv. Funct. Mater.* **2018**, *28*, 1801868.
8. D. Qi, L. Lu, L. Wang, J. Zhang, *J. Am. Chem. Soc.* **2014**, *136*, 9886-9889.
9. I. Alessandri, *J. Am. Chem. Soc.* **201**3, *135*, 5541-5544.
10. Y. Shin, J. Song, D. Kim, T. Kang, *Adv. Mater.* **2015**, *27*, 4344-4350
11. L. Jiang, T. You, P. Yin, Y. Shang, D. Zhang, L. Guo, S. Yang, *Nanoscale* **2013**, *5*,2784-2789.
12. D. Yan, W. Qiu, X. Chen, L. Liu, Y. Lai, Z. Meng, J. Song, Y. Liu, X. Liu, and D. Zhan, *J. Phys. Chem. C.* **2018**, *122*, 14467−14473
13. S. G. Park, C. Mun, M. Lee, T. Y. Jeon, H. S. Shim, Y. J. Lee, J. D. Kwon, C. S. Kim, D. H. Kim, *Adv. Mater.* **2015**, *27*, 4290-4295.
14. S. Su, C. Zhang, L. Yuwen, J. Chao, X. Zuo, X. Liu, C. Song, C. Fan, L. Wang, *ACS Appl. Mater. Interfaces* **2014**, *6*, 18735.
15. D. Maznichenko, K. Venkatakrishnan, B. Tan , *J. Phys. Chem. C* **2012** , *117* , 578 .